Hindawi
Advances in Civil Engineering
Volume 2018, Article ID 4738628, 14 pages
https://doi.org/10.1155/2018/4738628

Research Article

The Liquefaction Behavior of Poorly Graded Sands Reinforced with Fibers

Eyyüb Karakan,[1] **Tuğba Eskişar**,[2] **and Selim Altun**[2]

[1]*Department of Civil Engineering, Geotechnical Division, Kilis 7 Aralik University, Kilis, Turkey*
[2]*Department of Civil Engineering, Geotechnical Division, Ege University, İzmir, Turkey*

Correspondence should be addressed to Eyyüb Karakan; eyyubkarakan@gmail.com

Received 1 August 2017; Revised 6 January 2018; Accepted 10 January 2018; Published 15 March 2018

Academic Editor: Arnaud Perrot

This study focuses on the performance of fibers, improving the resistance to liquefaction in loose sands, medium sands, and dense sands in Izmir, Turkey. A systematic testing schedule consisting of cyclic triaxial tests was held under stress-controlled and undrained conditions on saturated sand specimens with and without fiber reinforcements. The major parameters having effects on the dynamic behavior such as fiber content, fiber length, and relative density on the liquefaction behavior and the excess pore water pressure developments of specimens with and without fibers were investigated. If the fiber content or the fiber length was increased in the specimens, higher number of loading cycles was needed in order to experience the liquefaction of sands. The reinforcement effect in medium-dense specimens was found to be apparently distinctive compared to loose specimens. The curves of pore water pressures and shear strains were achieved for the fiber-reinforced sands. The boundaries of pore water pressure curves presented in the literature on the clean sands were utilized in comparison with the pore water pressure curves of fiber-reinforced sands of this study. As a conclusion, the results presented in this study are useful to develop insight into the behavior of clean and fiber-reinforced sands under seismic loading conditions. Based on the test results, it was found that the number of loading cycles had a strong impact on the excess pore pressure generation.

1. Introduction

The liquefaction phenomenon in a layer of loose sand under dynamic circumstances occurs by the development of excess pore water pressure and decrement of average effective stress which corresponds to a complete loss of shear strength. Liquefaction may cause damages due to bearing capacity loss of strata, large settlements, tilting of structures, and lateral displacements. Condition of soil could be improved by reinforcement to eliminate the liquefaction hazard. Using reinforcement materials such as fibers in soil medium may provide an alternative to reduce the liquefaction potential. Compared to conventional improvement methods using reinforcement, fibers have some advantages like prevention of potential weak planes which mostly form parallel to plane oriented reinforcement and conservation of isotropic shear strength characteristics [1]. The reinforced soil behavior of fibers was studied by researchers in the last decades, but focusing the problem only under static conditions [2–5]. It was revealed that using fiber reinforcement in soil increased the shear strength of soil and improved the ductile behavior and reduced the strength loss observed after the peak strength was achieved. Recently, static liquefaction studies explored the possibility of fiber reinforcement to improve the liquefaction resistance of sand. These studies stated that the occurrence of lateral spreading could be prevented by using fiber reinforcement [6, 7].

Wave propagation during the earthquakes originates undrained shear stresses in the soil medium, the particles of soil experience shear strains, and the pore water pressures are generated in the soil medium. Development of excess pore water pressure decreases the stiffness in response to an applied overburden pressure and triggers a vicious circle that causes larger shear strains and higher pore water pressures.

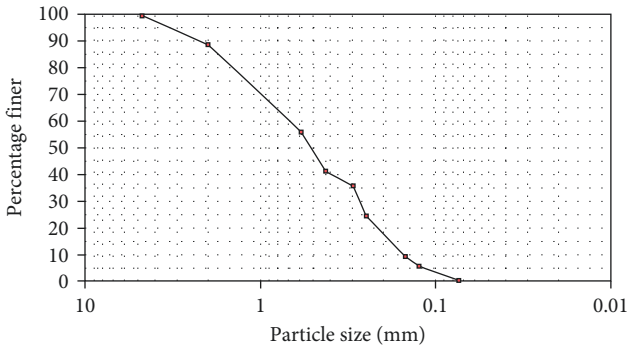

Figure 1: Grain-size distribution of the sand.

(a)

(b)

Figure 2: Materials used in this study. (a) 6 mm PP fibers. (b) 12 mm PP fibers.

Table 1: Test cases conducted in this study.

Relative density (D_r) (%)	Fiber length (FL) (mm)	Fiber ratio (FR) (%)
30/50/70	Without	
	6	0.25
		0.50
		1.00
	12	0.25
		0.50
		1.00

At the final stage, the excess pore water pressure reaches a level of initial overburden pressure, and liquefaction is initiated. Since 1970s, analyzing and modelling of excess pore water pressures in soils under earthquake excitations gained interest among the researchers of geotechnical earthquake engineering. In this paper, along with the findings of this study, other literature is also reviewed and compared with the results provided by the experiments. A detailed testing program is followed by conducting experiments on clean sand specimens with varying conditions by using the cyclic triaxial compression testing device. The results of experimental sets are evaluated by stress-based methods, main parameters affecting the behavior and the uncertainties are considered during analyses, and practical solutions are compared with the existing models.

Over the last years, the effects of applying reinforcement materials to increase the shear strength of sands and the factors, including reinforcement type and reinforcement material, soil gradation, and reinforcement dispersion, have been studied only under static conditions by monotonic loadings [8–13]. Studies by Consoli et al. [4] and Consoli et al. [14] focused on consolidated drained triaxial tests to examine the fiber reinforcement effect on the mechanical behavior of sand admixed with varying cement content. Specimens with a relative density of 70% were prepared, and empirical equations to determine peak and residual strength based on cement content, fiber content, and confining pressure were proposed in Consoli et al. [4] and Consoli et al. [14]. The resistance to liquefaction in fiber-reinforced soils increased the number of cycles required to cause liquefaction under undrained loading conditions [15–20]. Cyclic triaxial test results have indicated that the shear modulus of reinforced soil is not only under the control of shear strain, but also under the control of many factors such as fiber content, loading repetition, and confining pressure [21]. Bhandari and Han [22] worked on the interaction between the geotextile and the soil under a cyclic wheel load applying the discrete element method. The results showed that the geotextile depth had a major effect on the degree of interaction between the geotextile and the soil. Shuai-dong and Xiang-juan [23] examined the cyclic behavior of reinforced silty sand by performing consolidated undrained cyclic triaxial tests. The dynamic elastic modulus of reinforced soil was reported to increase due to reinforcement, confining pressure, and consolidation stress ratio, as to the unreinforced soil. The literature is mainly focused on the resistance of soils against liquefaction, but pore water pressure development is a very effective sign of behavioral change which is mostly left out of the scope [24].

The aim of this study is to identify the liquefaction resistance and the pore water pressure development of fiber-reinforced sand specimens by applying cyclic triaxial tests. The majority of the previous studies have explored the strength and deformation properties of fiber-reinforced soil under monotonic loading conditions; this study particularizes the effectiveness of fibers in the liquefaction resistance improvement of poorly graded sand through some series of dynamic testing. The influence of fibers on the dynamic behavior is investigated in reinforced sand specimens. The sets of experiments included specimens with 0%, 0.25%, 0.5%, and 1% polypropylene fiber contents.

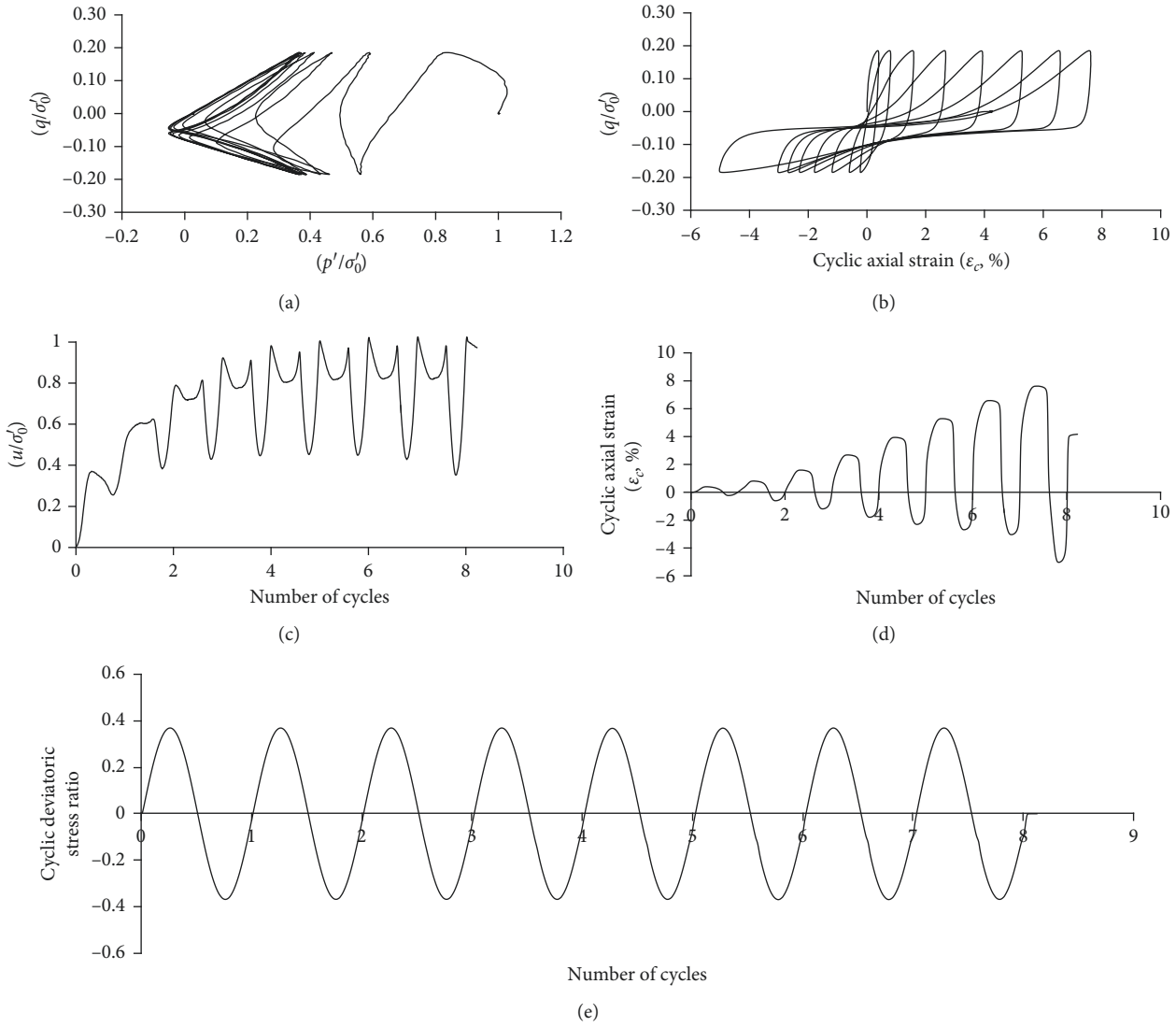

Figure 3: (a) Development of stress path. (b) Variation of stress path with cyclic axial strain. (c) Pore water pressure ratio with the number of cycles. (d) Cyclic axial strain with the number of cycles for a specimen of fiber-reinforced sand. (e) Cyclic deviatoric stress ratio with the number of cycles for a specimen of fiber-reinforced sand ($D_r = 30\%$, fiber length = 12 mm, fiber ratio = 0.25%, and $\sigma_0' = 100$ kPa).

Furthermore, the effect of fiber length is investigated by using two different fibers with lengths of 6 mm and 12 mm. The relative density of the specimens was 30%, 50%, and 70%, representing the different stiffness states of the soil. The specimens were consolidated under a confining pressure of 100 kPa, and a cyclic loading frequency of 0.1 Hz was applied. The variations of pore water pressure ratios with number of loading cycles, with fiber content, and with fiber length under constant stress amplitudes are achieved and presented in this study.

2. Materials and Testing Methods

2.1. Materials. A clean sand mass was obtained from an excavation site in the city center of Izmir, Turkey. The classification of the sand showed that it was poorly graded sand (SP) according to the Unified Soil Classification System. The effective size (D_{10}), the diameter corresponding to 30% finer (D_{30}), mean grain size (D_{50}), and the diameter corresponding to 60% finer (D_{60}) of the sand gradation were 0.15 mm, 0.28 mm, 0.53 mm, and 0.70 mm, respectively. The coefficient of uniformity was 4.67, and the coefficient of curvature was 0.75. The maximum void ratio of the sand was 0.84, and the minimum void ratio of the sand was 0.56. The specific gravity of the sand was 2.67. The grain-size distribution of this sand is shown in Figure 1. The relevant ASTM standards were followed for all index tests (ASTM D6913, ASTM D4253, ASTM D4254, and ASTM D854) [25–28].

The monofilament polypropylene (PP) fiber materials used in this study were also produced in Turkey by a local company. The fibers were rectangular in cross section with a specific density of 0.91. The tensile strength of fibers was 400 MPa, and elastic modulus of fibers was 1000–2500 MPa. Fiber lengths were 6 and 12 mm (Figure 2). Fiber ratios of 0.25%, 0.5%, and 1% were added to the specimens by dry weight of sand. Fiber-reinforced sand specimens were

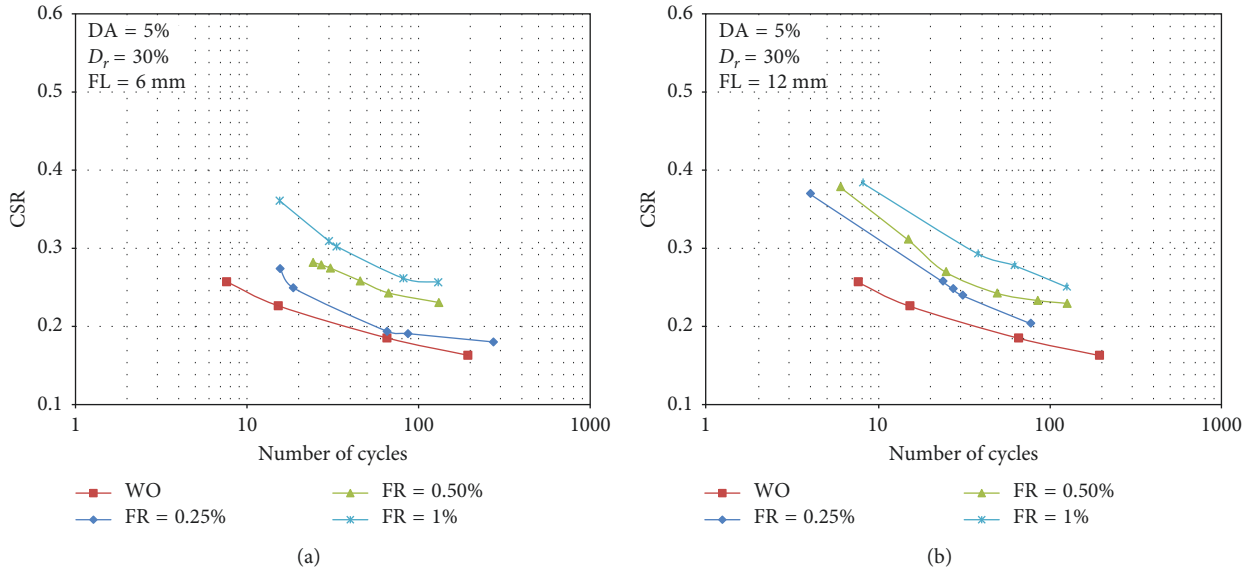

Figure 4: Variation of CSR with the number of cycles considering the effect of fiber length (a) FL = 6 mm and (b) FL = 12 mm (WO: without fibers, FR: fiber ratio, $D_r = 30\%$, and $\sigma_0' = 100$ kPa).

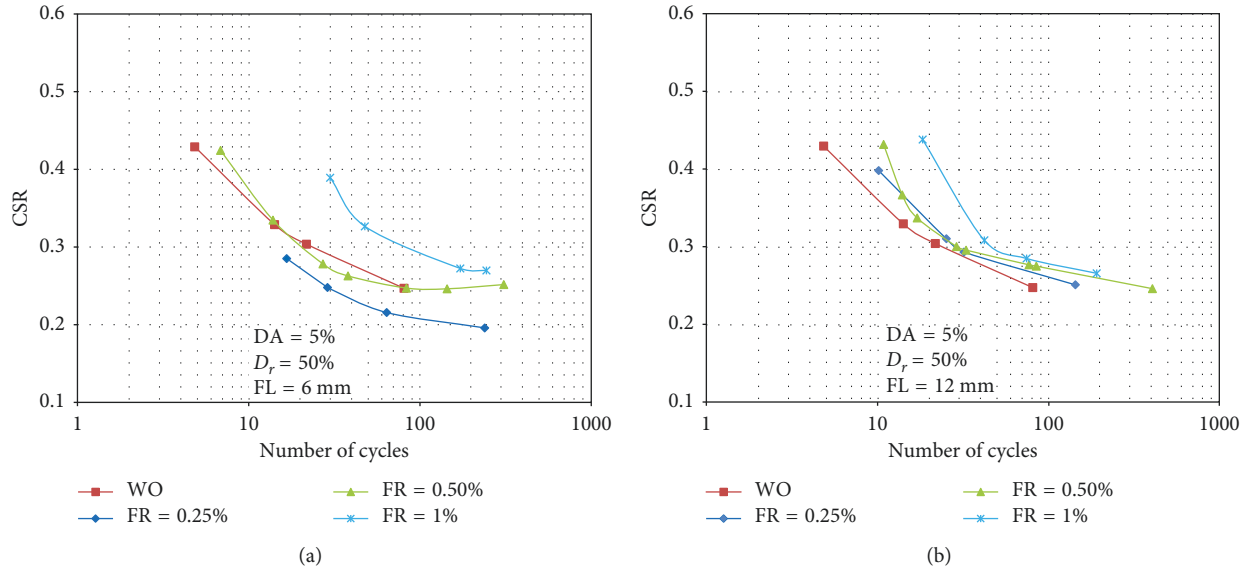

Figure 5: Variation of CSR with the number of cycles considering the effect of fiber length (a) FL = 6 mm and (b) FL = 12 mm (WO: without fibers, FR: fiber ratio, $D_r = 50\%$, and $\sigma_0' = 100$ kPa).

prepared at the same dry density as that of unreinforced sand. The percentage of fibers mixed with sand was calculated as a part of the total solids in the void-solid matrix of the sand. The amount of fibers added was calculated over the dry mass of sand.

2.2. Testing Program. A testing schedule was planned to investigate the effect of fiber reinforcement in sand specimens. The test cases were combinations of relative density of the sand, fiber length, and fiber ratio (Table 1). In addition to the planned schedule, some randomly chosen test cases were repeated to check the validation of specimen preparations of same relative density and loading conditions to demonstrate the accuracy of the test results.

2.3. Specimen Preparation. The initial specimen diameter was 50 mm, and specimen height was 100 mm in the experiments. The so-called "undercompaction technique" of Ladd [29] was adopted as the specimen preparation procedure. A porous stone and a circular filter paper were embedded in the base part of the testing device. A membrane made of rubber was placed in the base, and the movement of the membrane was prevented with O-rings. A

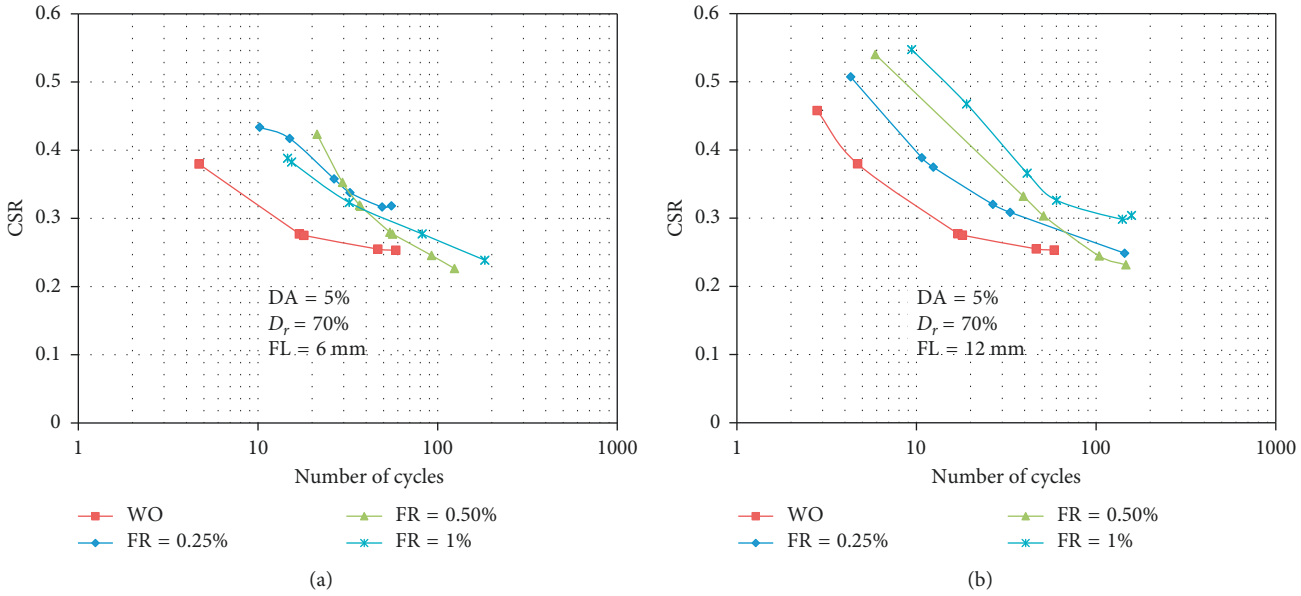

Figure 6: Variation of CSR with the number of cycles considering the effect of fiber length (a) FL = 6 mm and (b) FL = 12 mm (WO: without fibers, FR: fiber ratio, $D_r = 70\%$, and $\sigma_0' = 100$ kPa).

split mold was placed on the lower plate of the triaxial cell; after that, vacuum was applied to the mold. The upper part of the membrane was fitted tightly to the mold. A soil composite of dry sand and fibers was prepared and transferred to the mold step by step. The soil composite was divided into ten equal parts, and each part was carried into the mold. A wooden rod was used for compaction. In order to achieve sufficient bonding, top of every compacted layer was cleared off before locating the following layer. Another circular filter paper and a porous stone were set above the top of the specimen. The membrane was slipped to the specimen cap from the mold carefully. JGS 0520-2000 [30] was followed for the preparation of the specimens. The dynamic testing procedure of JGS 0541-2000 [31] was followed.

2.4. Test Procedure. The stress-controlled cyclic triaxial tests were performed. The triaxial testing system includes a vertical pressure loading unit with air and water panel, a triaxial cell, a pneumatic sine loader, an electric measurement unit, including, pressure, displacement, and volume change transducers, strain amplifiers, and a dynamic data acquisition system.

The specimens were initially flooded with carbon dioxide; after this step, the specimen was flooded with deaired water, and back pressure was applied to saturate the specimens. Skempton (B) parameter defining the saturation was assured to vary between 0.96 and 1.00. The specimens were isotropically consolidated under 100 kPa of effective stress, and undrained cyclic loading was subsequently applied in a stress-controlled manner. In the liquefaction tests, the loading sequence applies a certain number of cycles necessary to reach a specified level of cyclic stress under a frequency of 0.1 Hz until the specimen develops a double-amplitude (DA) axial strain of 5%. During cyclic loading, continuous digital data were recorded for the following parameters: cyclic axial strain (ε_c), excess pore water pressure (u), and the cyclic deviator stress ratio applied to the specimen. JGS 0541-2000 considers two criteria to define liquefaction. If the amplitude of cyclic axial load is relatively large, the number of cycles needed to cause liquefaction is accepted as the number of cycles needed to reach a maximum value of excess pore water pressure equal to 95% of the effective confining stress; otherwise, it is recognized as the number of cycles needed to reach a double amplitude of 5% of the axial displacement of the specimen. The experiments progress until all specimens reach 10% of the axial displacement.

Figure 3 shows the cyclic trixial test results of sand specimen prepared at a relative density of 30%. An effective confining pressure of 100 kPa was applied to the specimen. Figure 3(a) illustrates the development of the stress path of the specimen. During cyclic testing, a continuous sequence of compression and extension loadings having the same intensity was regularly applied to simulate dynamic conditions, which was seen from the steady change of q/σ_0' between +0.20 and −0.20. Figure 3(b) illustrates the variation of the stress path with the cyclic axial strain. The initial stage of the test started with a small cyclic axial strain, but as the applied cycles progressed, the strains became more dominant on the compression side to a level of 8% strain. Pore water pressure development with the number of loading cycles is given in Figure 3(c). A steady trend was observed in the progress of the pore water pressure ratio with the number of cycles. After 3 cycles, the liquefaction criterion was satisfied, and the cyclic axial strains varied over a wider range. Figure 3(d) shows the state when the pore water pressure ratio equals the effective pressure. Strain levels of +8% and −5% were achieved in the

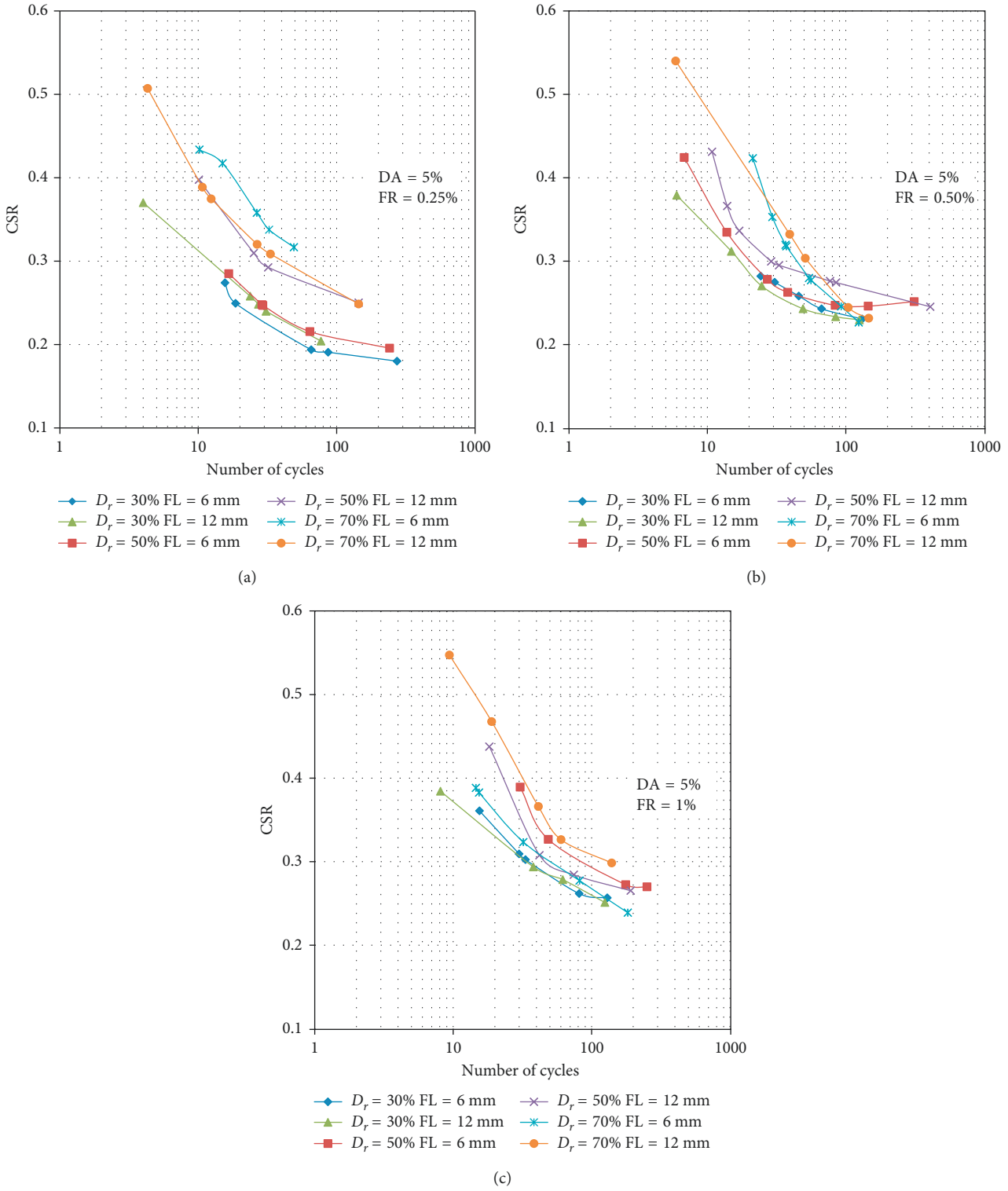

Figure 7: Variation of CSR with the number of cycles considering the effect of fiber ratio (a) FR = 0.25%, (b) FR = 0.50%, and (c) FR = 1% ($\sigma_0' = 100$ kPa).

compression and extension sides, respectively, resulting in a total strain of 13%. Figure 3(e) shows the cyclic deviator stress ratio with the number of cycles as an example of a measured record during undrained cyclic triaxial testing.

3. Results and Discussion

The main parameters of this study, namely, relative density, fiber length, and fiber ratio on the liquefaction resistance, are presented and discussed. It should be noted that all the

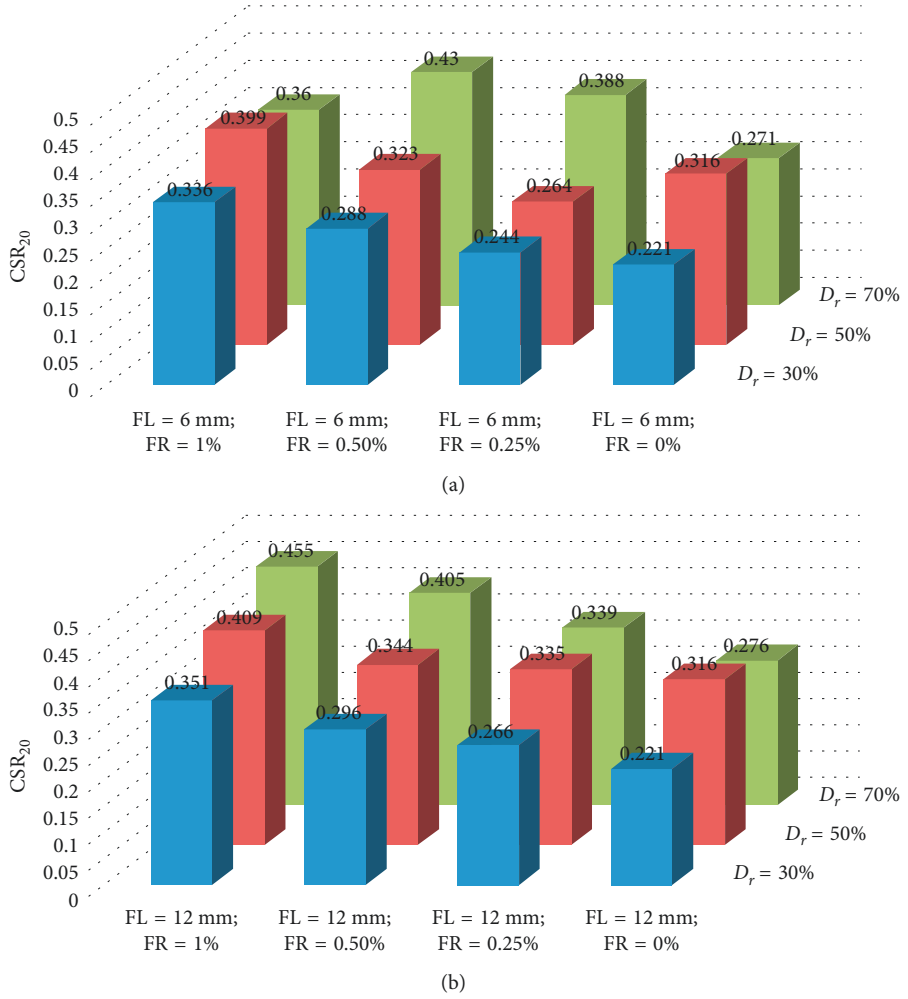

Figure 8: Cyclic stress ratio (CSR) values corresponding to $N_{cyc} = 20$ loading cycles. (a) FL = 6 mm. (b) FL = 12 mm.

outcomes of this study belongs to the experiments which were performed under 100 kPa effective confining pressure. The liquefaction criterion of the tests was to achieve the number of cycles when the specimen developed a double-amplitude (DA) axial strain of 5%.

3.1. Effect of Relative Density. The cyclic stress ratio is calculated as the cyclic strength normalized by the effective stress. In Figures 4–6, variations of the cyclic stress ratio (CSR) with the number of cycles of fiber-reinforced soils with relative densities of 30%, 50%, and 70% are shown, respectively. The control group consisting of specimens without fibers was also prepared in aforementioned relative densities and tested. Their results could also be viewed in Figures 4–6. An increase in fiber length increases the number of cycles that would trigger liquefaction for the specimens having a relative density of 30%. For specimens having a relative density of 50% and fiber length of 6 mm, lowest liquefaction resistance was obtained from specimens having a fiber ratio of 0.25%. Figure 4 shows the specimens constituted by using 6 mm fibers with sand and compacted to a relative density of 30% resulted a CSR value of 0.361 and the specimens prepared by using 12 mm fibers with sand and compacted to a relative density of 30% resulted a CSR value of 0.384. If the relative density was increased to 50%, a CSR value of 0.424 was found for the specimens with 6 mm fibers and a CSR value of 0.438 was found for the specimens with 12 mm fibers (Figure 5). When the relative density was attained as 70%, the CSR values corresponding to 6 mm and 12 mm were 0.434 and 0.547, respectively (Figure 6). In order to compare the variation of number of cycles with CSR values, the upper boundary of CSR was taken as 0.6. If Figures 4–6 were interpreted amongst themselves, the relative density was found the dominating factor among other variables such as fiber length and fiber ratio. It was seen that the maximum CSR values were obtained for specimens with 12 mm fibers and compacted to a relative density of 70%, resulting in the maximum resistance to liquefaction cycles [19, 20].

The specimens with a fiber ratio of 0.5% and the ones without fibers showed a similar liquefaction resistance. The highest resistance was achieved in specimens that contain 1% of fibers. For specimens having a relative density of 50% and fiber length of 12 mm, liquefaction resistance of specimens that contain no fiber, 0.25%, and 0.5% showed

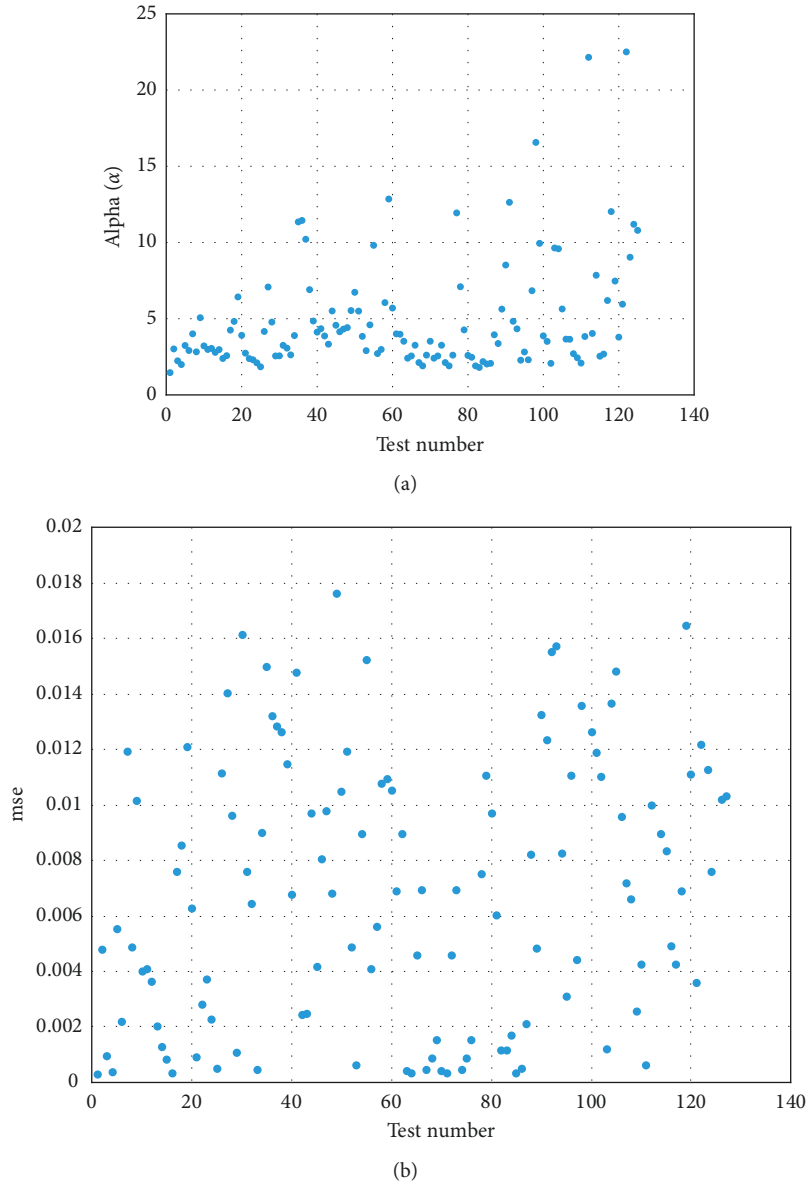

Figure 9: All (a) alpha (α) and (b) mse coefficients calculated by using the model proposed by Seed et al. [32].

a liquefaction resistance varying in a narrow band. The most remarkable improvement against liquefaction was obtained in specimens with 1% fiber content. For medium dense specimens, the effective length of fiber required to develop shear strength increased with the increase in fiber length at a constant fiber ratio. In this condition, the slippage taking place between individual fibers was reduced with fiber length increment, resulting in improved performance of fibers in soil.

3.2. Effect of Fiber Ratio. The fiber ratios of specimens were chosen as 0.25%, 0.5%, and 1.0%. For all test cases, the liquefaction resistance was highest for specimens with $D_r = 70\%$ and FL = 12 mm, and it was lowest for specimens with $D_r = 30\%$ and FL = 6 mm (Figure 7). This finding is valid for all fiber ratios used in this study. Besides, medium dense specimens ($D_r = 50\%$) with a fiber length (FL) of 6 mm showed the second best performance against liquefaction. This trend is followed in the same manner by loose specimens. This finding is associated with the fact that the voids in the soil matrix are covered by the fiber addition, inducing an additional densification of the solid matrix. This finding is in congruence with the results of Ibraim et al. [6].

3.3. Effect of Fiber Length. The cyclic stress ratios corresponding to 20 loading cycles at 5% double-amplitude axial strain are given in Figure 8. When the effect of fiber length is observed for fiber-reinforced specimens, CSR values are greater for longer fibers (FL = 12 mm). As an example, CSR is 0.264 for medium dense specimens having a fiber ratio of 0.25 and fiber length of 6 mm (Figure 8(a)), and CSR is 0.335 for medium dense specimens ($D_r = 50\%$) having a fiber ratio

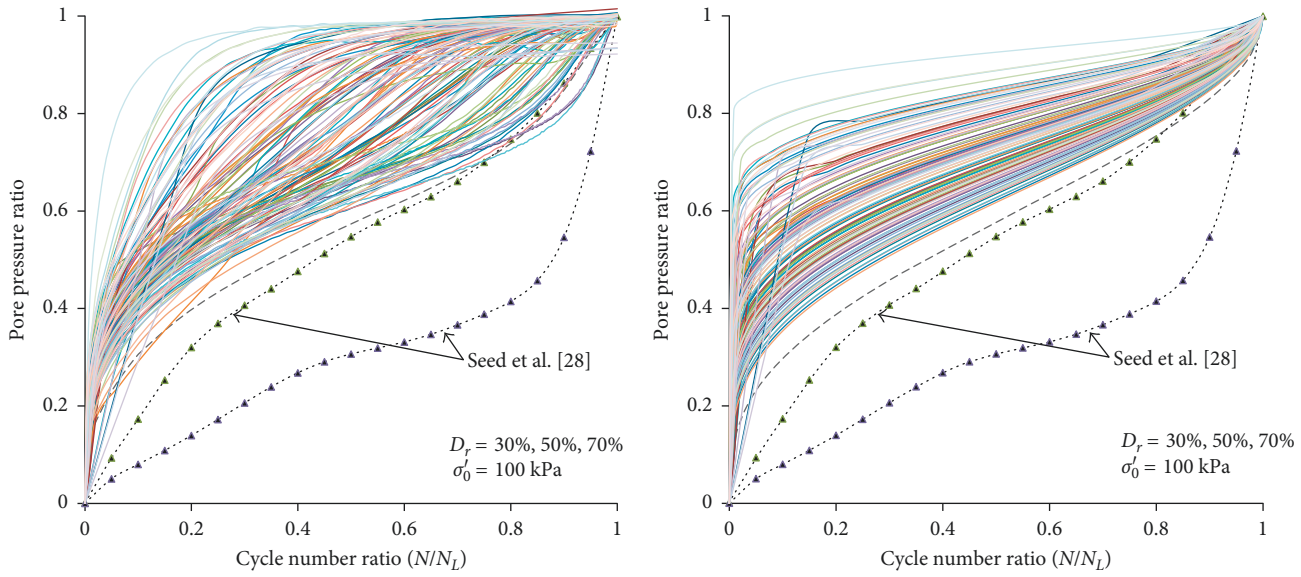

Figure 10: (a) Pore-water pressure ratio (PWP) versus cycle ratio number (N/N_L) obtained from the results of experiments. (b) Pore-water pressure ratio (PWP) versus number of cycles ratio (N/N_L) obtained by using α coefficients from the model proposed by Seed et al. [32].

of 0.25 and fiber length of 12 mm (Figure 8(b)). The increase in CSR is 27%. Therefore, it may be said that the fiber length increment also improves the liquefaction resistance of the poorly graded sand. If a comparison is made between loose specimens with fiber ratios of 0% and 1%, improvement in liquefaction resistance is 52% for loose specimens that contain 6 mm long fibers, and improvement in liquefaction resistance is 59% for loose specimens that contain 12 mm long fibers. A notable development in liquefaction resistance is observed when the poorly graded sand is reinforced with fibers.

3.4. Pore Pressure Development. In liquefaction tests, the pore water pressure develops continuously and reaches the initially applied confining stress after a certain amount of loading cycles. Pore water pressure generation depends on the relative density of the soil and the existing cyclic stress ratio. In addition, shear strain of the soil is a dominating property that relates to the effect of number of loading cycles on the level of pore water pressure. Since four decades, an interest has been raised to evaluate the generation of excess pore water pressure of sands considering the above mentioned parameters, and some numerical models were proposed in literature. However, the behavior of reinforced soils is still not clear and requires further research.

In this section, the main parameters of this study, namely, relative density, fiber length, and fiber ratio on the pore water pressure generation curves, are presented and discussed. It should be noted that all the outcomes of this study belong to the experiments which were performed under 100 kPa effective confining pressure. The liquefaction criterion of the tests was to achieve the number of cycles when the specimen developed 5% double-amplitude axial strain.

In order to model the pore water pressure generation in fiber-reinforced specimens, two different stress-based models were considered, and α coefficients of these models are achieved by calculating the smallest mean square error in each model.

The model proposed by Seed et al. [32] can be stated in a closed-form solution in

$$r_u = \left\{\frac{1}{2} + \frac{1}{\pi}\sin^{-1}\left[2*\left(\frac{N}{N_{\text{liq}}}\right)^{1/\alpha} - 1\right]\right\}, \quad (1)$$

where r_u is the pore water pressure ratio, N is the number of equivalent uniform loading cycles, and N_{liq} is the number of cycles required to produce initial liquefaction ($r_u = 1.0$). α is a function of the soil properties and test conditions.

In this study, the model offered by Seed et al. [32] is used to evaluate the pore-water pressure ratio data. α coefficients are calculated with a confidence interval of 95% by using the bootstrapping, which allows assigning measures of accuracy to specimen estimates of fiber-reinforced sand specimens. α coefficients are presented as individual points along with all specimen data. α coefficients versus test numbers are given in Figure 9. α coefficient calculated with a confidence interval of 95% was found as 4.920 in Figure 9 [24].

The relationship between the pore-water pressure ratio and number of cycles required to initiate liquefaction for the specimens having 30%, 50%, and 70% relative densities which were consolidated under 100 kPa of overburden pressure are given in Figure 10. Figure 10(a) shows the curves where pore-water ratio values are normalized with the number of cycles ratio values, while Figure 10(b) shows

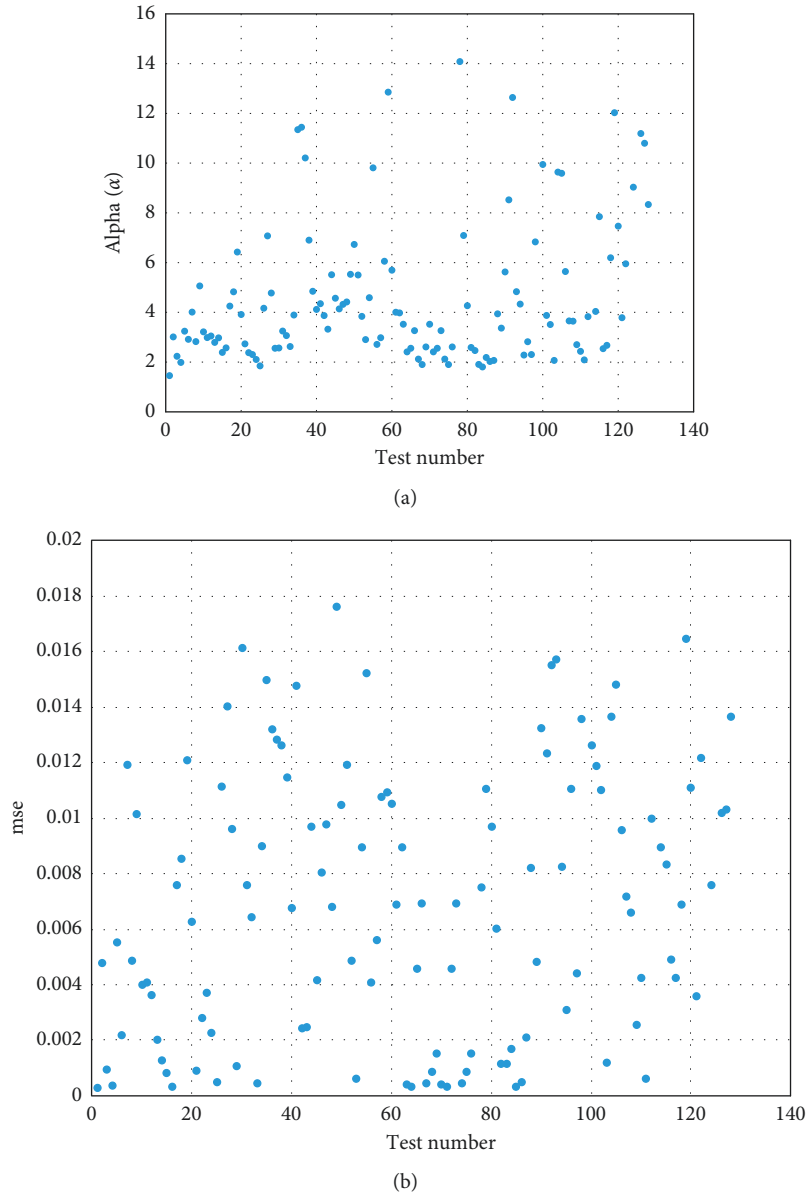

Figure 11: All (a) alpha (α) and (b) mse coefficients calculated by using the model proposed by Booker et al. [33].

the curves obtained by calculating the smallest mean square error for α coefficient and using (1). α coefficient is 4.92 on the average, which is higher than the upper limit value offered in the work of Seed et al. [32]. In Figure 10(a), it is seen that when the pore-water pressure ratio is 30%, the number of cycle ratio is 10%. However, if (1) is used to calculate α coefficients, then the pore-water ratio becomes 50% from the same point where the number of cycles ratio is 10% (Figure 10(b)). As α coefficients are highly dependent on soil conditions, fiber-reinforced medium resulted in much higher α coefficients, which is depicted as curve arcs with steep slopes, than the curves observed for the clean sands.

Booker et al. [33] proposed another equation (2) similar to the pore-water pressure model proposed by Seed et al. [32].

$$r_u = \left\{ \frac{2}{\pi} \sin^{-1} \left[\frac{N}{N_{\text{liq}}} \right]^{(1/2*\alpha)} \right\}. \quad (2)$$

Model parameters such as r_u, N, N_{liq}, and α have the same definitions with (1). α coefficients are calculated with a confidence interval of 95% by using the bootstrapping methodology to provide comparison with the results of Seed's equation. α coefficients are presented as individual points along with lower limit, average, and upper limit values of all specimen data in Figure 11.

The same procedure explained in methodology of Seed et al. [32] is also followed for the model suggested by Booker et al. [33] to derive the curves of pore-water pressure ratio-number of cycles ratio. α coefficient is derived as 3.66. Figure 12(a) shows the curves where pore-water ratio values are normalized with the number of cycles ratio values, while

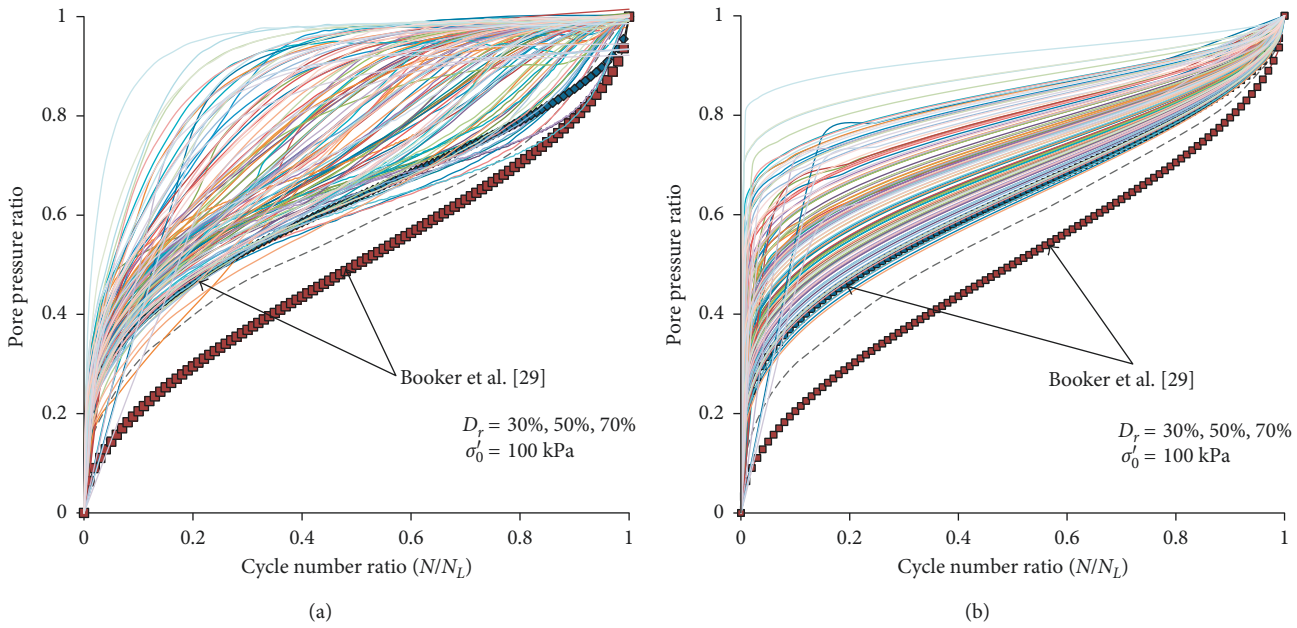

Figure 12: Pore-water pressure ratio (PWP) versus cycle ratio number (N/N_L) (a) obtained from the results of experiments and (b) obtained by using α coefficients from the model proposed by Booker et al. [33].

Figure 12(b) shows the curves obtained by calculating the smallest mean square error for α coefficient and using (2). For the initial 10–20% of number of cycles ratio, the pore water pressure development is relatively quick, and pore pressure ratio is in the range of 50–60%.

A statistical evaluation of methodology of Seed et al. [32] was performed by Polito et al. [34]. According to Polito et al. [34], it was concluded that the model coefficient (α) should be estimated as a function which includes the variables of cyclic stress ratio (CSR), fines content of the soil (FC), and relative density of the soil (D_r):

$$\alpha = \alpha_1 * \mathrm{FC} + \alpha_2 * D_r + \alpha_3 * \mathrm{CSR} + \alpha_4. \quad (3)$$

In this study, the finer passing through number 200 mesh was around 0.14%, therefore α_1 could be neglected. Using the bootstrap algorithm, α_2, α_3, and α_4 values were calculated as 2.230, 1.757, and 3.222, respectively, and their dispersion among with the tests are given in Figure 13.

Pore-water pressure ratio (PWP) versus number of cycles ratio (N/N_L) obtained from the results of the experiments are shown in Figure 14(a). Figure 14(b) shows pore-water pressure ratio (PWP) versus number of cycles ratio (N/N_L) obtained by using α coefficients in (3) by the bootstrap method of the model proposed by Polito et al. [34]. The number of cycles ratio of 0.2 corresponds to a PWP of 50%. By using (3), minimizing all mean square errors was possible, and for every α coefficient, pore water pressure versus number of cycles ratio could be obtained (Figure 14(b)). High values of α coefficients were calculated; this means high pore water pressure values were produced in the beginning number of cycles ratio in conformity with Figure 14(b). The critical point was 50% of pore pressure where the number of cycles ratio was 0.1.

3.5. Effect of Double Amplitude (DA) of Axial Strain. The effect of number of loading cycles on the pore pressure level is basically a shearing strain function [35]. The change of double-amplitude axial strain with the number of cycles in each testing condition with corresponding cyclic stress ratio (CSR) is given in Figure 15.

Liquefaction occurred instantly in reinforced sand specimens with lower relative densities; because of this, double amplitude of axial strain follows a perpendicular path (Figure 15(a)). The values of CSR bigger than 0.230 required number of cycles less than 20 to observe liquefaction. As the CSR decreased, the number of cycles to liquefaction increased. In Figure 15(b), at a constant CSR value of 0.286, the number of cycles to liquefaction was 14 for specimens with 0.25% of fibers, 16 for specimens with 0.50% of fibers, and 33 for specimens with 1% of fibers. Increment of fiber ratio dramatically increased the number of cycles at a constant value of CSR. This finding proves the efficiency of fiber ratio in sand specimens. Fiber ratio has a direct effect on the number of cycles resulting in liquefaction in reinforced specimens.

4. Conclusions

A series of dynamic experiments was carried out by performing cyclic triaxial tests on poorly graded sand specimens. The sand was obtained in bulk form in an excavation site in Izmir-Turkey. The liquefaction and stress-strain behavior of the sands were investigated in laboratory triaxial tests performed on reconstituted specimens. The confining pressures were 100 kPa reflecting the actual overburden pressure in situ conditions. The frequency of testing was held at 0.1 Hz. Three different relative density values of the sand were considered: loose (D_r = 30%), medium dense (D_r = 50%), and dense (D_r = 70%). The parameters affecting

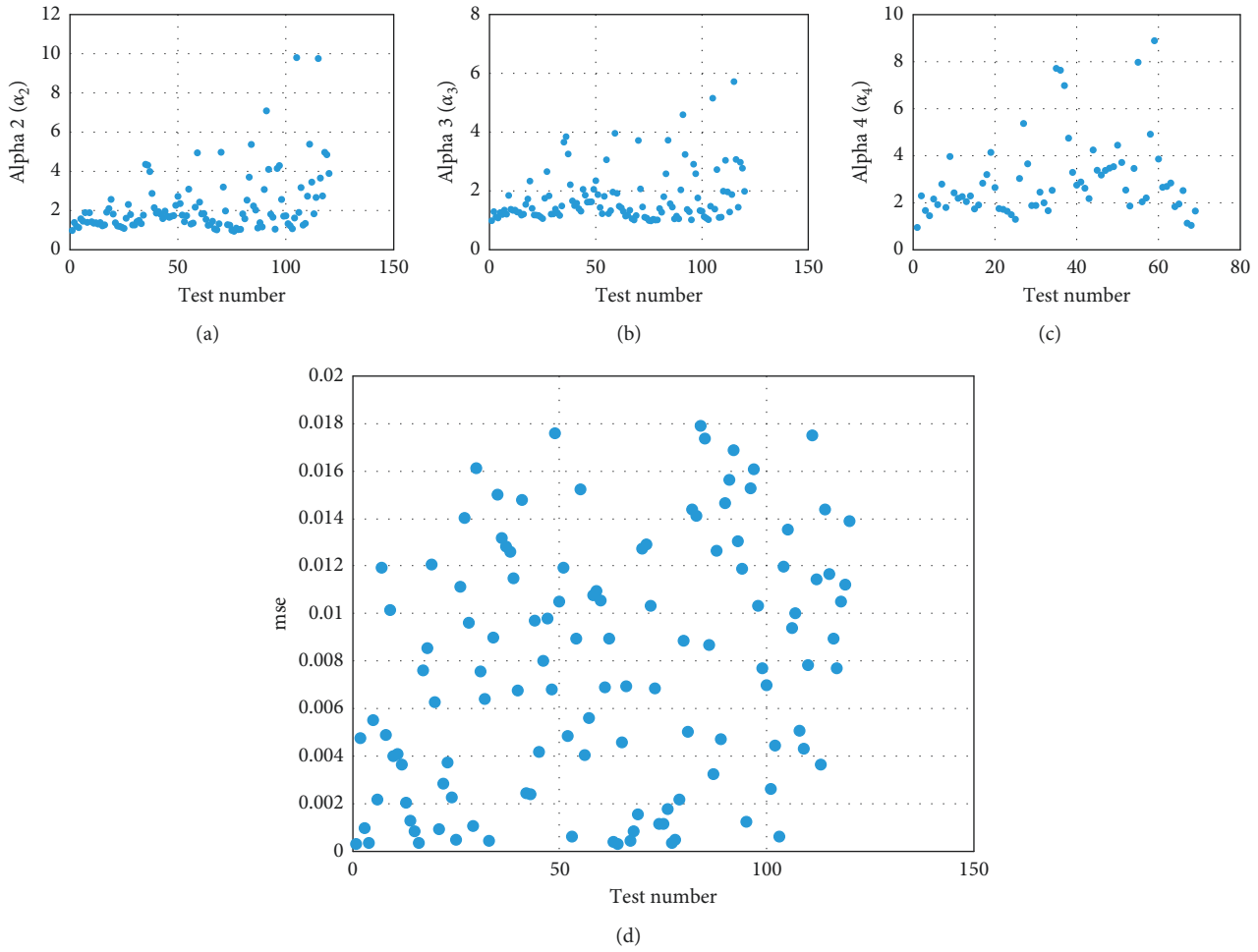

Figure 13: All (a) alpha (α) and (b) mse coefficients calculated by using the model proposed by Polito et al. [34].

the liquefaction behavior of soil were considered as fiber content (0.25%, 0.50%, and 1%), fiber length (6 mm and 12 mm), and relative density. Specimens without fibers were also prepared and tested as a control group in the relative densities of 30%, 50%, and 70%. Liquefaction behavior was observed and explained through cyclic stress curves, and the excess pore water pressure developments of specimens with and without fibers were modeled with the relevant equations in the literature, and model parameters considering the effect of fibers were proposed. The following conclusions could be summarized in this study:

(1) The fiber existence causes a major change in the liquefaction behavior and reduces the susceptibility of soil to liquefy. If the fiber ratio was increased, the number of cycles triggering liquefaction was also increased. Maximum improvement in resistance to liquefaction was for sand specimens reinforced with 1% fibers at $D_r = 50\%$, and FL = 12 mm. The results apparently imply that fiber reinforcement could be an effective solution improving the liquefaction resistance of the poorly graded sand.

(2) CSR values increased with the increment of fiber length. This result is attributed to the development of a better mesh structure in the soil matrix as more grains can interrelate with a longer fiber.

(3) The liquefaction resistance of the poorly graded sand increases with an increase in relative density. In medium dense specimens ($D_r = 50\%$), the reinforcement effect was found to be distinctive compared to the loose specimens ($D_r = 30\%$).

(4) In this study model parameter (α), mean square error of α coefficients are obtained for the pore water pressure models offered by Seed et al. [32] and Booker et al. [33]. Mean square errors of both models were assured to be less than 0.02.

(5) Seed et al. [32] and Booker et al. [33] were preferred due to the similar nature and to provide comparison to the findings of this study. The accuracy of the models of Seed et al. [32] and Booker et al. [33] are checked by mean square errors. These values were found very close to each other. However, the experimental results of fiber-reinforced sand specimens showed that α coefficient is affected from the relative density of the reinforced medium, cyclic shear strength ratio, and the properties of fibers such as length and ratio. Obtaining higher coefficients for the reinforced soil should be interpreted in this manner.

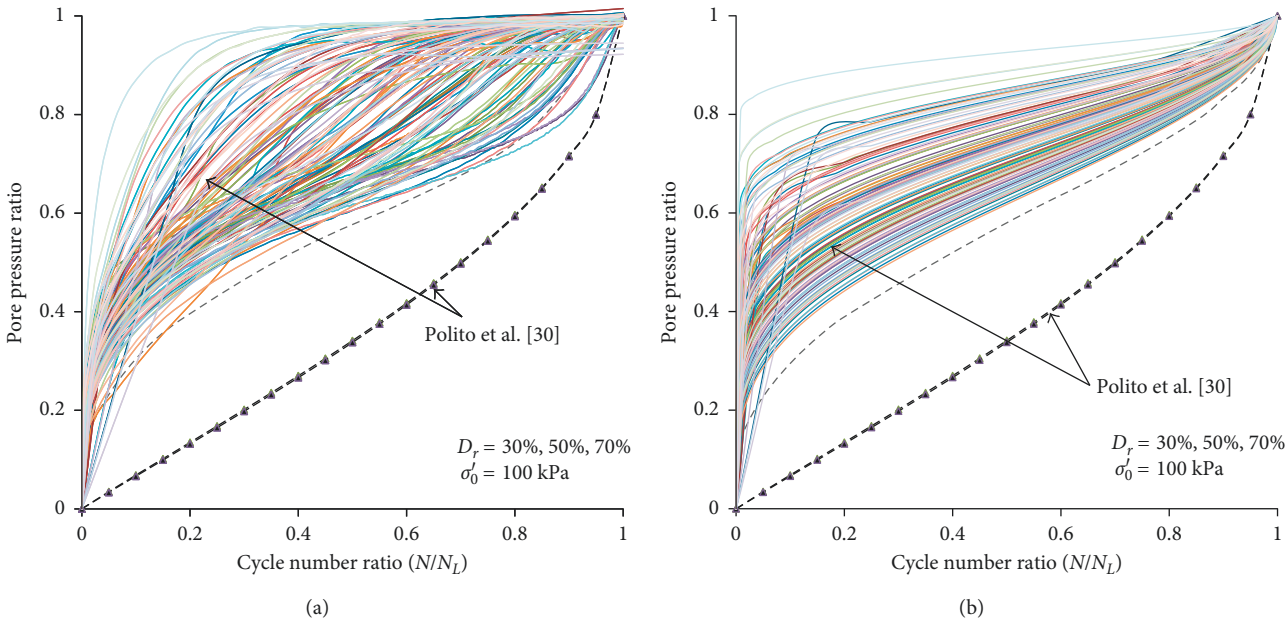

Figure 14: Pore-water pressure ratio (PWP) versus cycle ratio number (N/N_L) (a) obtained from the results of experiments and (b) obtained by using α coefficients from the model proposed by Polito et al. [34].

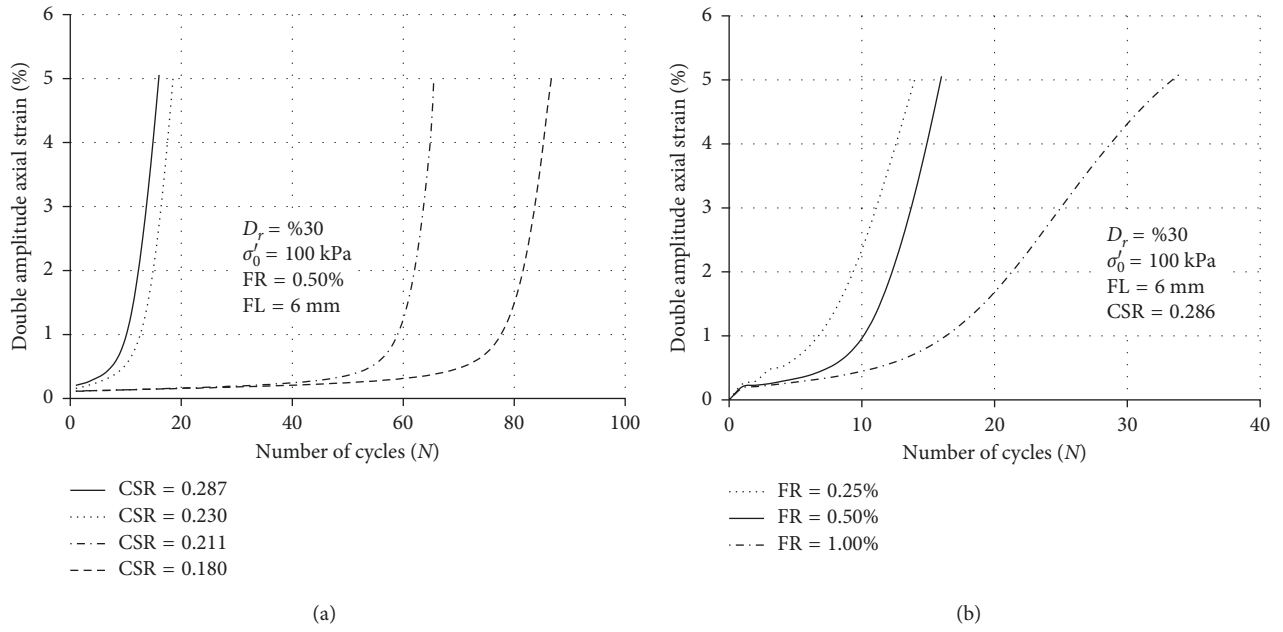

Figure 15: Variation of double-amplitude axial strain with number of loading cycles for reinforced sand. (a) Comparison of CSR values. (b) Comparison of fiber ratio.

(6) Statistical calculations depending on the fiber length, fiber ratio, and CSR values are compared with the statistical model offered by Polito et al. [34]. In this method, fines content is taken as 0%. The statistical parameters showed that fiber length, fiber ratio, and relative density of the medium highly affect and change the development of pore water pressure.

(7) Fiber reinforcement could be an alternative in lowering or eliminating the lateral movement of the sands caused by liquefaction. Further research is planned to focus on lateral spreading of fiber-reinforced poorly graded sand.

Conflicts of Interest

The authors declare that there are no conflicts of interest regarding the publication of this paper.

References

[1] M. H. Maher and D. H. Gray, "Static response of sand reinforced with randomly distributed fibers," *Journal of Geotechnical Engineering*, vol. 116, no. 11, pp. 1661–1677, 1990.

[2] N. R. Krishnaswamy and N. T. Isaac, "Liquefaction analysis of saturated reinforced granular soils," *Journal of Geotechnical Engineering*, vol. 121, no. 9, pp. 645–651, 1995.

[3] D. Vercueil, P. Billet, and D. Cordary, "Study of the liquefaction resistance of a saturated sand reinforced with geosynthetics," *Soil Dynamics and Earthquake Engineering*, vol. 16, no. 7-8, pp. 417–425, 1997.

[4] N. C. Consoli, M. D. T. Casagrande, A. R. Thome, M. Fahey, and F. Dallarosa, "Effect of relative density on plate loading tests on fibre-reinforced sand," *Géotechnique*, vol. 59, no. 5, pp. 471–476, 2009.

[5] S. Sadek, S. S. Najjar, and F. Freiha, "Shear strength of fiber-reinforced sands," *Journal of Geotechnical and Geoenvironmental Engineering*, vol. 136, no. 3, pp. 490–499, 2010.

[6] E. Ibraim, A. Diambra, D. Muir Wood, and A. R. Russell, "Static liquefaction of fiber reinforced sand under monotonic loading," *Geotextiles and Geomembranes*, vol. 28, no. 4, pp. 374–385, 2010.

[7] J. Liu, G. Wang, T. Kamai, F. Zhang, J. Yang, and B. Shi, "Static liquefaction behavior of fiber-reinforced sand in undrained ring shear tests," *Geotextiles and Geomembranes*, vol. 29, no. 5, pp. 462–471, 2011.

[8] S. M. Haeri, R. Noorzad, and A. M. Oskoorouchi, "Effect of geotextile reinforcement on the mechanical behavior of sand," *Geotextiles and Geomembranes*, vol. 18, no. 6, pp. 385–402, 2000.

[9] M. G. Latha and V. S. Murthy, "Effects of reinforcement form on the behavior of geosynthetic reinforced sand," *Geotextiles and Geomembranes*, vol. 25, no. 1, pp. 23–32, 2007.

[10] E. A. Subaida, S. Chandrakaran, and N. Sankar, "Laboratory performance of unpaved roads reinforced with woven coir geotextiles," *Geotextiles and Geomembranes*, vol. 27, no. 3, pp. 204–210, 2009.

[11] C. Khoury, G. Miller, and K. Hatami, "Shear strength of unsaturated soil-geotextile interfaces," in *Proceedings of the GeoFlorida 2010*, pp. 307–316, West Palm Beach, FL, USA, February 2010.

[12] S. C. Tuna and S. Altun, "Mechanical behaviour of sand-geotextile interface," *Scientia Iranica*, vol. 19, no. 4, pp. 1044–1051, 2012.

[13] E. B. Altalhea, M. R. Taha, and F. M. Abdrabbo, "Bearing capacity of strip footing on sand slopes reinforced with geotextile and soil nails," *Jurnal Teknologi*, vol. 65, no. 2, 2013.

[14] N. C. Consoli, M. A. A. Bassani, and L. Festugato, "Effect of fiber-reinforcement on the shear strength of cemented soils," *Geotextiles and Geomembranes*, vol. 28, no. 4, pp. 344–351, 2010.

[15] N. M. Uzdavines, "Dynamic behavior of saturated sand reinforced with geosynthetic fabrics," in *Proceedings of the Conference of Geosynthetics '89*, pp. 385–396, California, San Diego, February 1989.

[16] M. H. Maher and R. D. Woods, "Dynamic response of sands reinforced with randomly distributed fibers," *Journal of Geotechnical Engineering*, vol. 116, no. 7, pp. 1116–1131, 1990.

[17] B. Maheshwari, H. Singh, and S. Saran, "Closure to "Effects of reinforcement on liquefaction resistance of Solani Sand"," *Journal of Geotechnical and Geoenvironmental Engineering*, vol. 139, no. 9, pp. 1634-1635, 2013.

[18] T. Eskisar, S. Altun, and E. Karakan, "Assessment of liquefaction behavior of Izmir sand reinforced with randomly distributed fibers," in *Proceedings of the 6th International Conference on Earthquake Geotechnical Engineering*, Christchurch, New Zealand, November 2015.

[19] T. Eskisar, E. Karakan, and S. Altun, "Effects of fiber reinforcement on liquefaction behavior of poorly graded sands," *Procedia Engineering*, vol. 161, pp. 538–542, 2016.

[20] T. Eskisar, E. Karakan, and S. Altun, "Effects of fiber-reinforcement on liquefaction behavior and pore pressure development of sand," in *Proceedings of the 12th International Congress on Advances in Civil Engineering (ACE 2016)*, İstanbul, Turkey, September 2016.

[21] J. Li and D. W Ding, "Nonlinear elastic behavior of fiber-reinforced soil under cyclic loading," *Soil Dynamics and Earthquake Engineering*, vol. 22, pp. 977–983, 2002.

[22] A. Bhandari and J. Han, "Investigation of geotextile-soil interaction under a cyclic vertical load using the discrete element method," *Geotextiles and Geomembranes*, vol. 28, no. 1, pp. 33–43, 2010.

[23] Y. Shuai-dong and Y. Xiang-juan, "The experimental study on the dynamic behavior of reinforced silty sand," in *Proceedings of International Conference on Electric Technology and Civil Engineering (ICETCE)*, pp. 2745–2750, Lushan, China, April 2011.

[24] E. Karakan, S. Altun, and T. Eskisar, "The pore water pressure behavior of sands reinforced with fibers," in *Proceedings of the Türkiye Deprem Mühendisliği ve Sismoloji Konferansı*, pp. 14–16, Izmir, Turkey, October 2015.

[25] ASTM D6913, *Standard Test Methods for Particle-Size Distribution (Gradation) of Soils Using Sieve Analysis*, ASTM International, 2017.

[26] ASTM D4253, *Standard Test Methods for Maximum Index Density and Unit Weight of Soils Using a Vibratory Table*, ASTM International, 2016.

[27] ASTM D4254, *Standard Test Methods for Minimum Index Density and Unit Weight of Soils and Calculation of Relative Density*, ASTM International, 2016.

[28] ASTM D854, *Standard Test Methods for Specific Gravity of Soil Solids by Water Pycnometer*, ASTM International, 2006.

[29] R. S. Ladd, "Preparing test specimens using undercompaction," *Geotechnical Testing Journal*, vol. 1, no. 1, pp. 16–23, 1978.

[30] JGS 0520-2000, *Preparation of Soil Specimens for Triaxial Tests*, Japanese Geotechnical Society, Japan, 2000.

[31] JGS 0541-2000, *Method for Cyclic Undrained Triaxial Tests on Soils*, Japanese Geotechnical Society, Japan, 2000.

[32] H. B. Seed, P. P. Martin, and J. Lysmer, "Pore water pressure change during soil liquefaction," *Journal of the Geotechnical Engineering Division*, vol. 102, no. 4, pp. 323–346, 1976.

[33] J. R. Booker, M. S. Rahman, and H. B. Seed, *GADFLEA: A Computer Program for the Analysis of Pore Pressure Generation and Dissipation During Cyclic or Earthquake Loading*, Rep. No. EERC 76–24, Earthquake Engineering Research Center, University of California, Berkeley, CA, USA, 1976.

[34] C. P. Polito, R. A. Green, and J. Lee, "Pore pressure generation models for sands and silty soils subjected to cyclic loading," *Journal of Geotechnical and Geoenvironmental Engineering*, vol. 134, no. 10, pp. 1490–1500, 2008.

[35] D. Erten and M. H. Maher, "Cyclic undrained behaviour of silty sand," *Journal of Soil Dynamics and Earthquake Engineering*, vol. 14, no. 2, pp. 115–123, 1995.